ORIGINAL ARTICLE

Running test on high-speed railway track-simply supported girder bridge systems under seismic action

Jian Yu[1] · Lizhong Jiang[1,2] · Wangbao Zhou[1,2] · Xiang Liu[1] · Leixin Nie[1] ·
Yuntai Zhang[1] · Yulin Feng[3] · Shanshan Cao[4]

Abstract

Considering that existing shaking table tests on bridge structures have not taken into account the effect of moving trains, this paper takes a multi-span simply supported girder with a CRTSII slab ballastless track system and a Chinese CRH2C high-speed train as its objects of study, builds a reduced-scale model for the bridge and train using a similarity ratio of 1:10, and constructs an on-bridge running test platform based on a four-array shaking table. A running test under seismic action is preformed to explore the effects of train speed and the vertical component of ground motion on structural responses under the combined action of seismic and train loads. According to the findings of this paper, a higher train speed leads to more intense wheel-rail interactions. Train speed and the vertical component of ground motion have significant effects on the vertical deformation of structures and on the transverse deformation of bearings and piers, but their effects on the transverse deformation of track structures are negligible. The vertical component of ground motion may cause vertical separation between girders and bearings. The train may induce disengaging between track structures in the vicinity of girder gaps.

Keywords Shaking table test · High-speed railway · Train speed · Vertical component of ground motion

---

Jian Yu and Lizhong Jiang have contributed equally to this paper.

✉ Wangbao Zhou
    zhouwangbao@163.com

1   School of Civil Engineering, Central South University, Changsha 410075, China

2   National Engineering Laboratory for High Speed Railway Construction, Changsha 410075, China

3   School of Civil Engineering and Architecture, East China Jiaotong University, Nanchang 330013, China

4   Guangdong Transportation Technology Testing Co., Ltd, Guangzhou, China

1 Introduction

To meet the strict ride comfort and stability requirements for high-speed railways (HSRs), current HSR construction extensively adopts the fully-enclosed construction practice of "building bridges as a substitute for roads". In recent years, HSR construction has extended to seismic fault zones in mountainous areas and high-seismic intensity zones in coastal areas. With increasing bridges and spans and the worsening of running environments, it is impossible for high-speed trains in high-density service to completely avoid riding on a bridge during an earthquake, either temporally or spatially. In order to ensure the safety of HSR bridge structures, examining their seismic responses under the combined action of seismic and train loads is of great theoretical significance and practical engineering value (Jiang et al. 2019a, b, c; Jiang et al. 2020a, b).

The shaking table test constitutes an essential part of aseismic test methods (Gao and Yuan 2019). Jiang et al. (2019a, b, c), by conducting a shaking table test on an HSR continuous girder bridge, explored the effects of different seismic intensities and loading directions on the seismic responses of structures and analyzed their damage states under seismic action. Yang et al. (2019) carried out shaking table tests on an HSR simply supported girder, aiming to investigate how the collision between anti-collapse systems and bearing pad stones would affect the seismic responses of the bridge and analyze the damping effect of rubber buffers. Zou et al. (2019) optimized the performance parameters of a novel isolation system and tested the reduced-scale specimens of an HSR bridge adopting the isolation system, thus verifying the working efficiency of the system. Jiang et al. (2019a, b, c) examined the working performance of friction pendulum bearings under seismic action by testing an HSR isolated simply supported girder bridge as well as selected and optimized dowel parameters on this basis. The sliding isolators were also discussed in references (Kumar et al. 2015; Barone et al. 2019; Furinghetti et al. 2019; Jangid, 2001; Pavese et al. 2019).

However, existing studies rarely explicitly consider the effect of the train, which is either ignored or regarded as pure additional static mass. After investigating the seismic responses of train-bridge systems, Du et al. (2012) pointed out the important influence of trains on the vertical vibration of HSR systems. Zhang et al. (2011) indicated that wheel-rail interactions would cause structural vibration, which would further superpose with earthquake-induced vibration, resulting in more significant structural responses. Liu et al. (2017), through comparing a single-bridge model with a train-bridge coupling model, discovered that there were significant differences between the two models in natural vibration characteristics and seismic responses, and that their difference in seismic response amplitude exceeded 20%. He et al. (2011) explored the effect of train-bridge interactions on the seismic responses of Japan's Shinkansen and revealed that, because of the damping effect of the train system, treating the train as a pure mass added to bridge structures would produce errors in the results. Kim and Kawatani (2006) made clear that the approach of taking the train as an additional mass would give excessively conservative results.

To solve the above problems, Wei et al. (2018a, b) introduced a reduced-scale train model prepared with a scale of 1:10 into a shaking table test on HSR double-track concrete simply supported box girders and studied the seismic responses of train-bridge systems. However, they failed to realize train movement in this test. On the basis of investigating the train-bridge system responses, Guo et al. (2012) pointed out that, due to the presence of track irregularities, the transverse displacement, vertical displacement, and acceleration of girders all increase with increasing train speed, and that train

speed served as an important factor influencing the vibration of train-bridge systems. According to the literature (Antolín et al. 2013; Zhang et al. 2010, 2011), train speed has a significant influence on the vibration of bridge structures caused by track irregularities, and neglecting the effect of train speed may lead to inaccurate results.

Considering that existing studies about shaking table tests of railway bridges rarely consider the effect of moving trains, it is necessary to conduct research, so as to more accurately simulate the seismic responses of HSR bridge structures under the combined action of seismic and train loads. Taking a multi-span simply supported girder with a CRTSII slab ballastless track system and a Chinese CRH2C high-speed train as its objects of study, this paper constructs an on-bridge running test platform based on a four-array shaking table at a geometric scale of 1:10, performs a running test under seismic action, and explores the effects of train speed and the vertical component of ground motion on structural responses under the combined action of seismic and train loads, offering a test basis for theoretical studies on the seismic responses of HSR bridge structures.

2 Test overview

2.1 Prototype HSR system

In this test, a multi-span simply supported girder with a CRTSII slab ballastless track system, located in an 8-degree seismic fortification zone in China, was analyzed, as shown in Fig. 1. The girders used in this test were C55 standard prestressed concrete box girders 32.5 m in length; the piers were C35 round-end solid piers with a section size of 2×6 m; and the bearings were pot rubber bearings with a vertical bearing capacity of 5,000 kN. The base plates were longitudinally full-length structures 2.55 m in width and 0.19 m in height. A 6 mm-thick sliding layer was paved between base plates and girders. The track slabs, 2.55×0.2 m in section size, were longitudinally continuous structures formed by linking longitudinal reinforcements on adjacent base plates using tensioning locks. A CA mortar layer 3 cm in thickness was placed between the track slabs and base plates. The rails were CHN60 rails using WJ-8C fastenings. The base plates, track slabs, and rails were made of C30 concrete, C55 concrete, and 71Mn steel, respectively. The shear grooves were set on the girder surface above the fixed bearings, and the shear reinforcements were set between the track slabs and base plates on both sides of the girder gaps. The lateral blocks were arranged with a spacing of 5.74 m. The HSR train was a Chinese CRH2C. See the main parameters of the train in Table 1 (Zhai et al. 2015), and the schematic of various prototype structures in Fig. 2 (Yu et al. 2020; Jiang et al. 2020a, b).
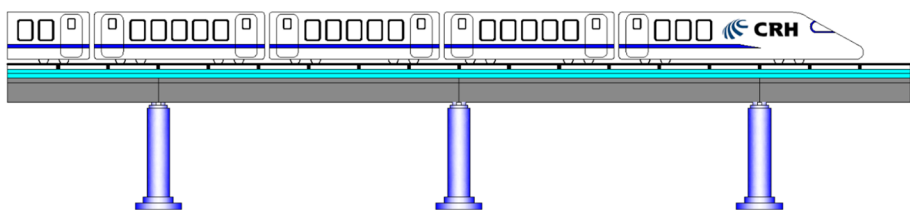

Fig. 1 Schematic diagram of the high-speed railway

Table 1 CRH2C train parameters

Property	Value	Unit
Distance between bogie centers	17.5	m
Bogie wheelbase	2.5	m
Car body mass	35,000	kg
Bogie frame mass	3,300	kg
Wheelset mass	1,800	kg
Primary and secondary suspension longitudinal stiffness	14,680 and 160	kN/m
Primary and secondary suspension transverse stiffness	6,470 and 160	kN/m
Primary and secondary suspension vertical stiffness	1,176 and 190	kN/m
Primary and secondary suspension longitudinal damping coefficient	0 and 5.06	kN·s/m
Primary and secondary suspension transverse damping coefficient	0 and 58.86	kN·s/m
Primary and secondary suspension vertical damping coefficient	5 and 39.87	kN·s/m

2.2 Test system

The entire test system consists of a shaking table system, a reduced-scale model, a train accelerator, a train decelerator, and a transition device (Fig. 3). The shaking table system (Fig. 4) is further composed of four 4 m × 4 m shaking tables, each of which can bear a maximum load of 30 t and provide a maximum horizontal acceleration of 1.0 g, a maximum vertical acceleration of 1.6 g, a maximum overturning moment of 30 t·m, and a maximum eccentric movement of 20 t m. The working frequencies of these shaking tables range between 0.1 and 50 Hz. The first shaking table is fixed, and the other three are movable. Each shaking table has 6 degrees of freedom (longitudinal, transverse, vertical, roll, yaw and pitch). Multi array digital control system is used in the laboratory, which can realize the synchronous output of seismic signals from different shaking tables. The control type of shaking tables is displacement control, which has a maximum working region length of 55 m and is applicable to aseismic tests on bridge structures.

To prepare a reduced-scale model (Fig. 5), the first step is to determine three control similarity ratios: geometric similarity ratio S_L; acceleration similarity ratio S_a; and material similarity ratio S_E. Considering that trains run fast on bridges to guarantee sufficient observation time, it is necessary to maximize the number of spans of the reduced-scale bridge model in the test region and to prevent an excessively small geometric similarity ratio from compromising specimen preparation precision. Based on these considerations, this test geometric similarity ratio S_L is 1/10. Train weight is an important influencing factor for train-bridge coupling, and gravity distortion should be avoided much possible in the shaking table test. For this reason, the acceleration similarity ratio S_a was set to 1 in this test. Given that there is a directly proportional relationship between specimen mass and material similarity ratio, to control specimen mass within the bearing capacity of shaking tables after determining S_L and S_a, the material similarity ratio S_E should be set as 1/2. After these three control similarity ratios are determined, other similarity ratios can be calculated according to the dimensional method (Jiang et al. 2019a, b, c) (Table 2). Based on the above similarity coefficient, the specimens were fabricated. See the schematic of the reduced-scale model in Fig. 5 and the materials parameters in Table 3. There are several points to be followed in the fabrication of the specimens: (1) For the convenience of specimen splicing and assembling, in this test, specimens were made of steel on the whole. (2)
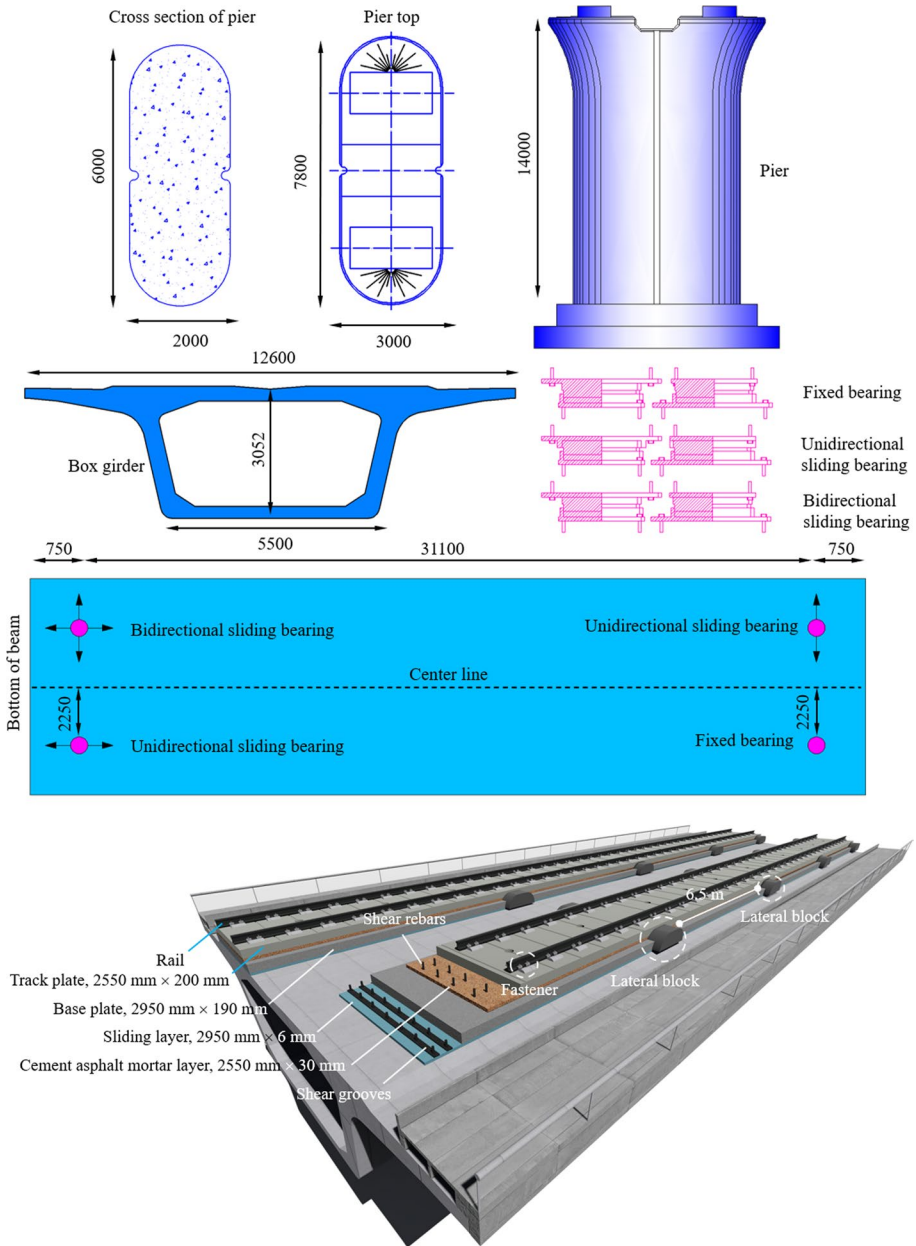
**Fig. 2** Schematic diagram of the prototype

The girders, piers, base plates, track plates, and rails tend to remain intact during earthquakes. Therefore, their nonlinearity was not taken into account in this experiment, and their reduced-scale models were fabricated using the principle of equivalent bending stiffness. The ratio of the bending stiffness of these specimens to the prototype is the stiffness similarity coefficient S_S. (3) The bearings, sliding layer, CA mortar layer, and fastenings,
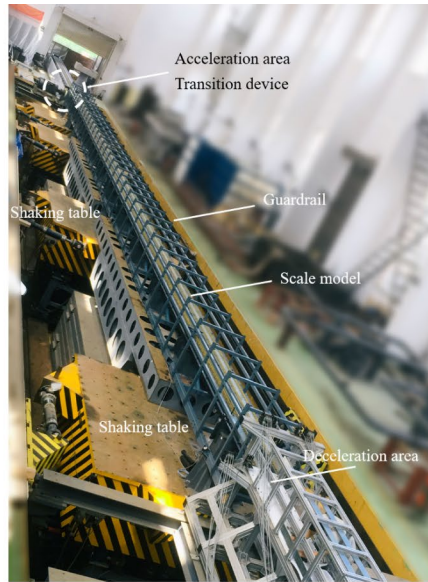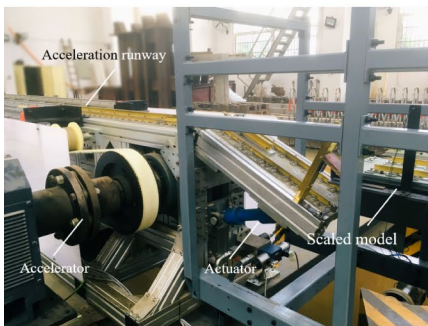
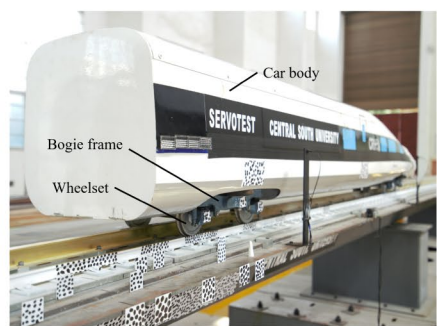**(a)** The shaking table system and the scaled bridge-track-train model
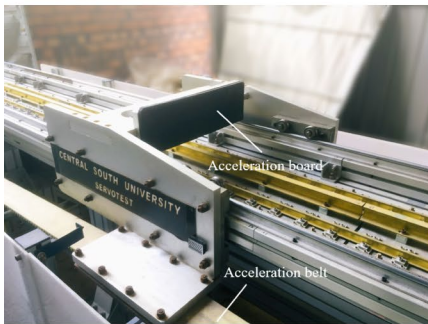
(b) Acceleration area
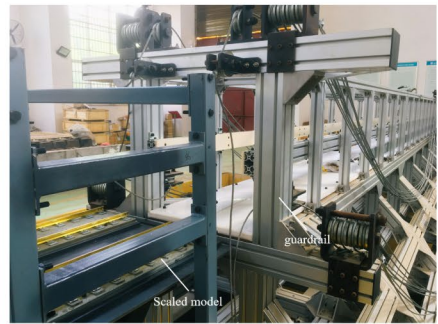
(c) Deceleration area

(d) Transition device

(e) Train model

Fig. 3 Schematic diagram of the shaking table test

DOFs: transverse, longitudinal, vertical, roll, yaw, pitch

Maximum bearing capacity: 30 ton

Maximum displacement: 0.25 m (horizontal) and 0.16 m (vertical)

Maximum acceleration: 1.0 g (horizontal) and 2.0 g (vertical)

Maximum anti-overturning moment: 30 ton·m
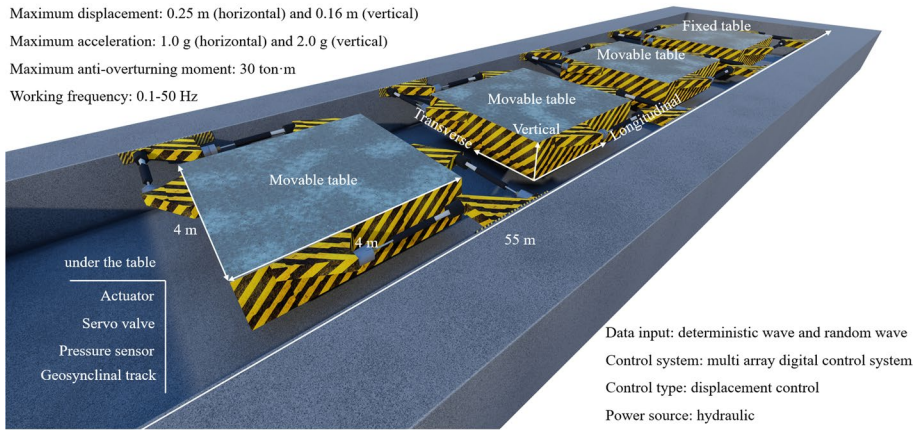
Working frequency: 0.1-50 Hz

Fixed table

Movable table

Movable table

Movable table

Transverse

Vertical

Longitudinal

4 m

4 m

55 m

under the table

Actuator

Servo valve

Pressure sensor

Geosynclinal track

Data input: deterministic wave and random wave

Control system: multi array digital control system

Control type: displacement control

Power source: hydraulic

Fig. 4 Schematic diagram of the laboratory

Bogie

Secondary suspension

Primary suspension

Wheelset

Fastener — Rail

Mortar layer — Track plate

Base plate

Sliding layer

Experimental similarity ratios

Geometric similarity ratio $S_L = 1/10$

Acceleration similarity ratio $S_a = 1$

Material similarity ratio $S_E = 1/2$

Mass similarity ratio $S_m = 1/200$

Density similarity ratio $S_\rho = 5$

Force similarity ratio $S_F = 1/200$

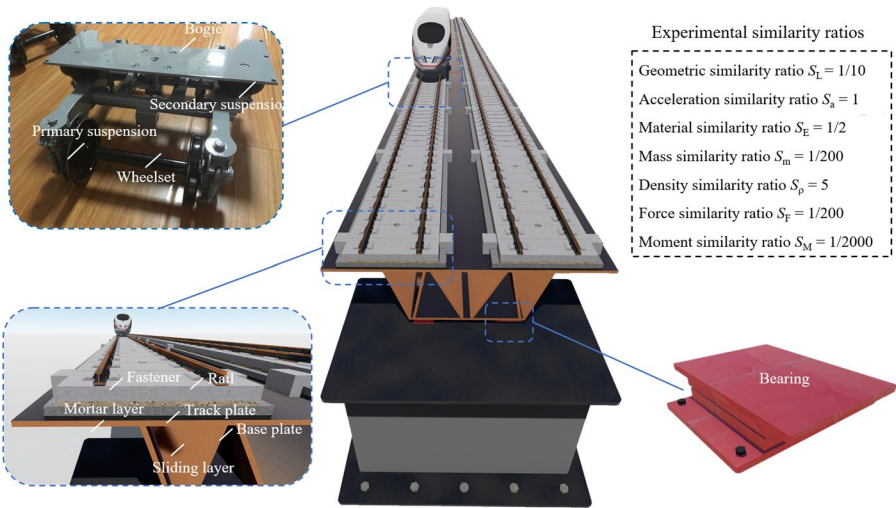Moment similarity ratio $S_M = 1/2000$

Bearing

Fig. 5 Schematic diagram of the specimens

serve important functions for the force transmission. Their nonlinearity was designed using the principle of equivalent force and displacement. The yield force and displacement of the specimens with different sizes were tested in the factory, and the size with the best similarity (S_F and S_L) to the prototype was adopted. (4) Shear reinforcements, shear grooves, and lateral blocks commonly experience no significant damage during earthquakes (Wei et al. 2016, 2017; Wei et al. 2018a, b); hence, they were designed be strong enough. (5) The train model was customized in the factory according to corresponding similarity ratios.

The acceleration area (Fig. 3b) and deceleration area (Fig. 3c), located on the two sides of the laboratory, are independent structures separated from the shaking table

Table 2 Experimental similarity factors

Physical parameter	Similarity factors	Similarity relation	Value
Length	S_L	S_L	1/10
Elastic modulus	S_E	S_E	1/2
Stress	S_σ	$S_\sigma = S_E$	1/2
Acceleration	S_a	S_a	1
Density	S_ρ	$S_\sigma / (S_a \cdot S_L)$	5
Mass	S_m	$S_\sigma \cdot S_L^2 / S_a$	1/200
Force or load	S_F	$S_\sigma \cdot S_L^2$	1/200
Moment	S_M	$S_\sigma \cdot S_L^3$	1/2000
Stiffness	S_S	S_F / S_L	1/20
Time	S_T	$S_L^{0.5} \cdot S_a^{-0.5}$	$1 / \sqrt{10}$
Velocity	S_V	$S_L^{0.5} \cdot S_a^{0.5}$	$1 / \sqrt{10}$

Table 3 Structural material parameters of the scaled model

Component	Materials	Component	Materials
Bridge	Steel (Q235)	Sliding layer	Polyurethane (ConipurM867F) and polyethylene
Pier	Steel (Q235)	CA mortar layer	Polyurethane (ConipurM867F)
Base plate	Steel (Q235)	Fastener	Steel (Q235) andVulcanized rubber
Track plate	Steel (Q235)	Shear rebar	Steel (Q420)
Rail	Steel (71Mn)	Shear slots	Steel (Q345)
Bearing	Steel (Q235) & PTFE	Lateral block	Steel (Q235)

system and the reduced-scale bridge model. The acceleration area consists of acceleration board, acceleration belt, accelerator and acceleration track. The accelerator pulls the acceleration board through the belt, and the train model is accelerated to test speed in the acceleration area.

The transition device (Fig. 3d) is located between the acceleration area and the model. The transition device consists of transition track and actuator. The position of the transition track can be adjusted by the actuator to connect or disconnect the acceleration area from the model.

The deceleration area consists of steel cage, buffering springs, and guardrail. When the train enters the deceleration area and is captured by the steel cage, the buffering springs between the cage and the guardrail reduce the train speed to zero.

At the beginning of this test, the train model first was accelerated to the test speed in the acceleration area and then entered the bridge model by way of the transition device. At the moment the train ran onto the bridge, the transition device was disconnected, the measurement system began to record, and the shaking tables began to apply seismic excitations until the train left the bridge and entered the deceleration area.

2.3 Measurement system

The measurement system consists of a VIC-3D high-speed camera system (Fig. 6) (manufactured by an American company, Correlatated Solutions Inc) and an IMC test system (manufactured by a Germany company, IMC test and measurement GmbH). The high-speed camera system is composed of two high-speed cameras, high-power lamps, and a speckle region pasted on specimen surface, which can capture structural displacement and deformation within the speckle region. The IMC test system is composed of acceleration sensors and a data collection system that can measure the structural acceleration.

High-speed cameras have a limited observation scope, and a maximum width of about 2 m, so selecting a reasonable observation region and suitable measurement indices is important. The seismic deformation of bridge structures is one of the core issues related to bridge safety, and track structures in the vicinity of girder gaps are more susceptible to earthquake-induced deformation and failure compared than other parts of the track. The deformation of bearings and piers is a focus of aseismic measures for bridges. Due to these considerations, the observation region was placed between the 5# girder and 6# girder in this test. Measurement indices included the deformation of track structures in the girder gap region, and the deformation of bearings and piers. In addition, for the purpose of studying the effect of the train on structures in the girder gap region, acceleration sensors were mounted at the end of the 5# girder and the top of the 6# pier. See the layout of speckle points and acceleration sensors in Fig. 7.

3 Seismic excitation

3.1 Design response spectrum

Chinese design response spectrum (Fig. 8a) was used to generate seismic excitation for the experiment. The determination of response spectrum requires the maximum horizontal acceleration α and periodic coefficient T_g, which can be referred to Tables 4 and 5.
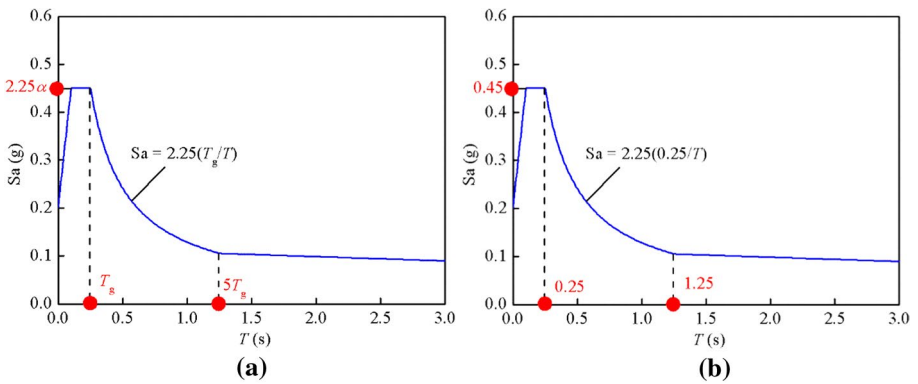
Based on the possibility and hazard intensity of earthquake occurrence, the seismic fortification zones in China are divided into 6, 7, 8, and 9-degree fortification zones, of

Fig. 6 VIC-3D high-speed camera system
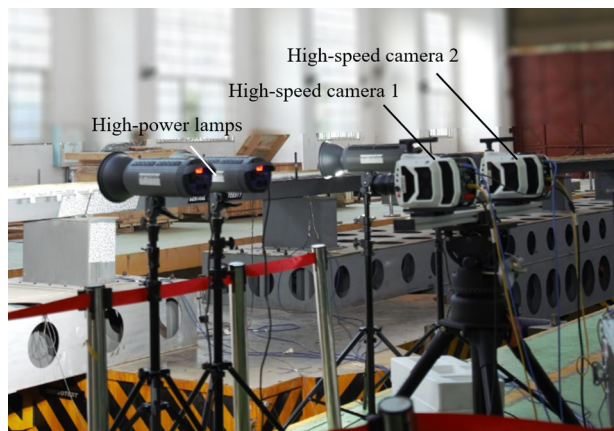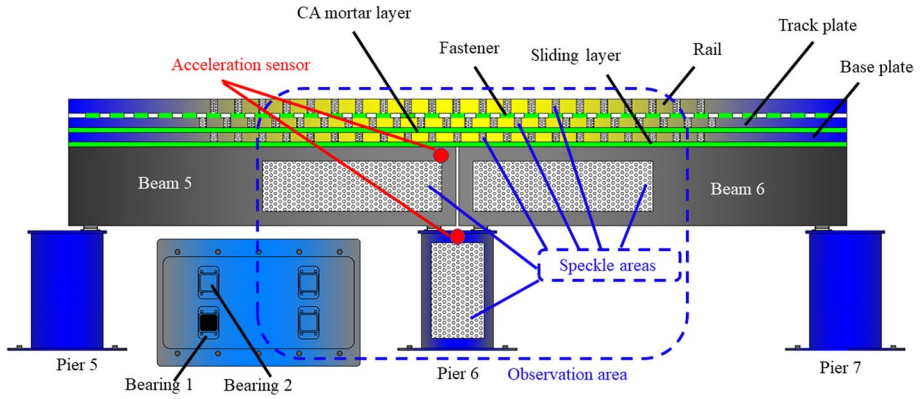
Fig. 7 Arrangement of speckle areas and acceleration sensors

Fig. 8 Chinese design response spectrum

Table 4 α under different earthquake levels

Earthquake level	Seismic fortification zones			
	6°	7°	8°	9°
Frequent earthquake	0.02 g	0.04 g	0.07 g	0.14 g
Fortification earthquake	0.05 g	0.10 g	0.20 g	0.40 g
Rare earthquake	0.11 g	0.21 g	0.38 g	0.64 g

Table 5 T_g under different site types

| Epicentral distance group	Site classification			
	Class I	Class II	Class III	Class IV
Group 1	0.25	0.35	0.45	0.65
Group 2	0.30	0.40	0.55	0.75
Group 3	0.35	0.45	0.65	0.90

which the maximum horizontal acceleration were shown in Table 4. In Table 5, the sites are divided into group 1, 2 and 3 according to the epicenter distance, and Class I, II, III, IV according to the soil type.

The protype bridge is located in an 8-degree seismic fortification zone in China, and the seismic excitation intensity of experiment was considered as fortification. Therefore, the α of response spectrum is 0.20 g. The site is a class-I and group-1 zone, and the T_g of response spectrum is 0.25 s. Hence, the design response spectrum (Fig. 8b) was established.
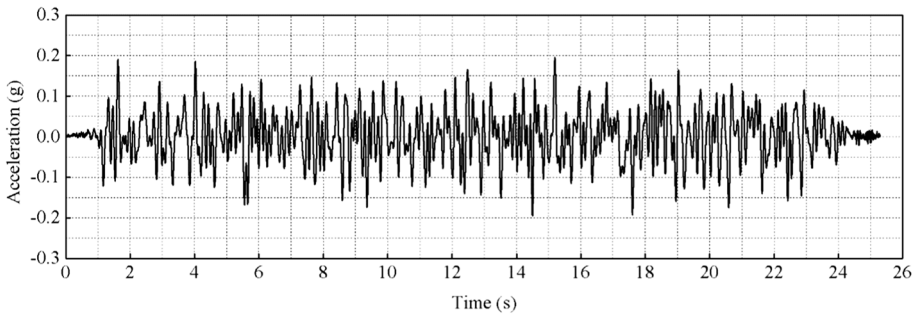
3.2 Acceleration time history curve

Limited by test conditions, if shaking tables were to move longitudinally, they might cause a collision between the bridge model and the transition device. Therefore, the ground motion input directions were set as transverse and vertical in this test. Chinese *code for seismic design of railway engineering* (Ministry of Railways of People's Republic of China 2009) stipulates that the vertical ground motion can be considered as a product of horizontal ground motion and coefficient k, and the coefficient k can be taken as 2/3.

SeismoArtif program was used to realize the conversion from response spectrum to acceleration time history curve (Fig. 9). The transverse experimental excitation of the shaking tables was obtained by multiplying the time axis of the prototype acceleration history
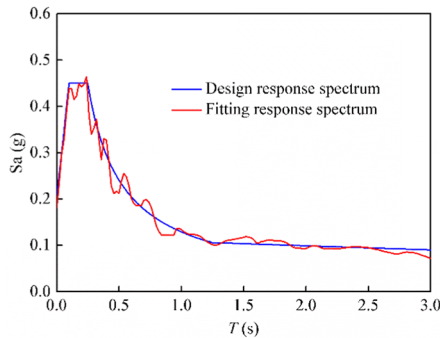
(a) Response spectrum of the acceleration time history

(b) Acceleration time history curve

Fig. 9 Seismic excitation of the prototype

by the time similarity ratio S_T (Fig. 10a). The vertical experimental excitation was obtained by multiplying the transverse seismic excitation by the coefficient 2/3 (Fig. 10b).

The output signals (Figs. 10c–d) of the shaking tables were collected, and their time axes were multiplied by the coefficient $1/S_T$ to generate the prototype response spectrum (Fig. 11). It can be seen that the response spectrums and time history curves of the input and output signals are generally close, indicating that the shaking table system can simulate the ground motion realistically.

4 Test analysis

4.1 Model dynamics

The natural frequency of the model bridge can be obtained by analyzing the power spectral density of its seismic response, which can be divided into following steps: (1) The shaking tables were used to apply white noise excitations to the model bridge, and the acceleration responses of 5# girder were recorded. (2) The acceleration responses were converted to acceleration power spectra density (Fig. 12). (3) The abscissas of the peak values for the power spectral density correspond to the natural frequencies of the model (Jiang et al. 2019a, b, c).

According to Fig. 12, the natural vibration frequencies of the first three orders of the bridge model's transverse modal shapes were 8.3 Hz, 11.3 Hz, and 16.0 Hz, respectively; the natural vibration frequencies of the first three orders of its vertical modal shapes were 23.1 Hz, 25.4 Hz, and 39.5 Hz, respectively. This suggests that the low-frequency component of ground motion can more easily excite transverse modal shapes of the bridge while the high-frequency component of ground motion can more easily excite vertical modal shapes.

4.2 Effect of train speed on the seismic responses of structures

### 4.2.1 Vertical seismic response

The bridge model is about 35 m in total length. In this test, it would take about 7 s and 3.5 s for the train to cross the bridge model at the speeds of 5 m/s and 10 m/s under seismic action, respectively. To ensure test precision, the high-speed camera shooting frequencies at 5 m/s and 10 m/s were set as 1000 FPS and 2000 FPS, respectively. Limited by the storage capacity of the high-speed cameras, the shooting durations at 5 m/s and 10 m/s were set as 6 s and 3 s, respectively. For the convenience of analyzing the effects of different speeds on the vertical seismic responses of structures, the first 3 s of the response time-history was intercepted for comparative analysis (Fig. 14) (where "0.2 g" means that the input transverse excitation peak value was 0.2 g, and "Y + Z" means that the transverse and vertical ground motion were applied at the same time). Figure 13 shows the test results of the IMC system, and Table 6 provides the maximum and minimum vertical seismic response of structures, where Max and Min denote the maximum and minimum seismic response, D_1 denotes the difference in the maximum response at different train speeds, D_2 denotes the difference in the minimum response, and D denotes the larger one of D_1 and D_2.

As can be seen from Fig. 13 and Table 6, the vertical girder-end acceleration of 5# girder showed significant pulses upon the arrival of the train (1.5–2 s and 3.5–4 s) even
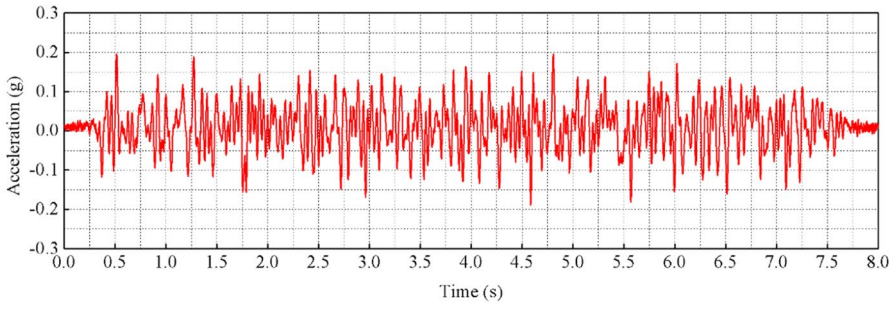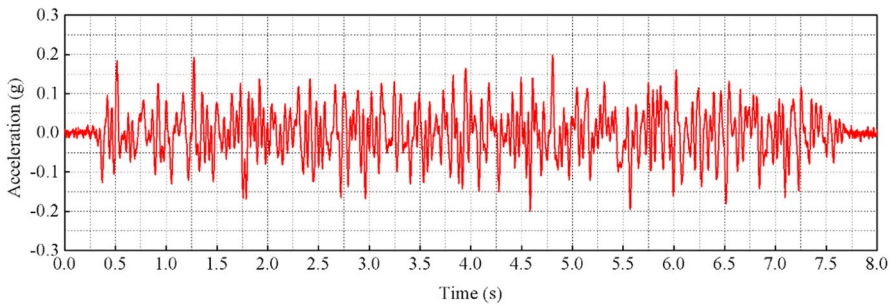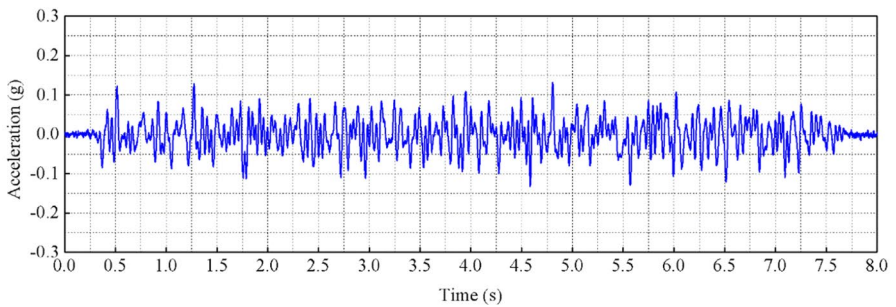
(a) Transverse, input signal
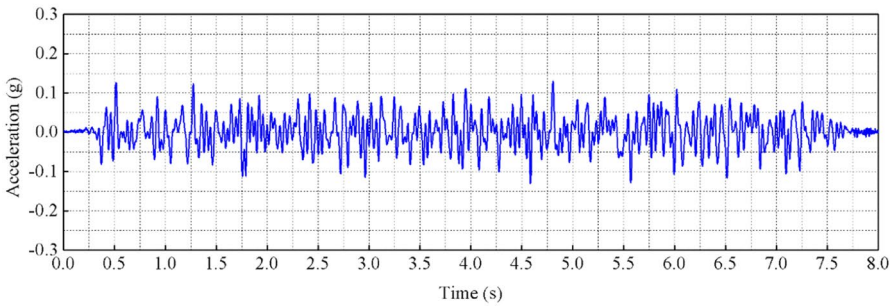
(b) Vertical, input signal

(c) Transverse, output signal

(d) Vertical, output signal

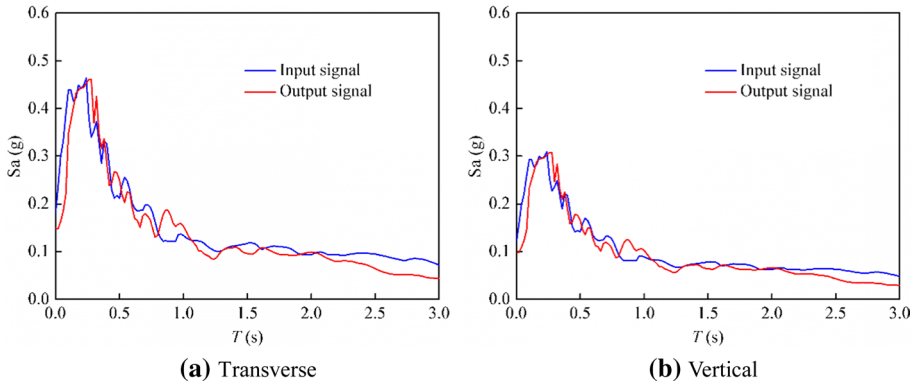**Fig. 10** Excitation signals of the shaking tables

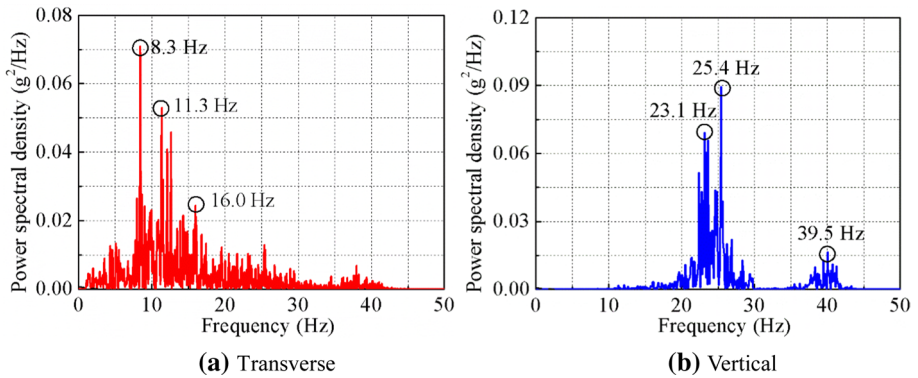**Fig. 11** Response spectrums of excitation signals of the shaking tables

Fig. 12 Vibration frequency of the scaled bridge model: (a) transverse; (b) vertical

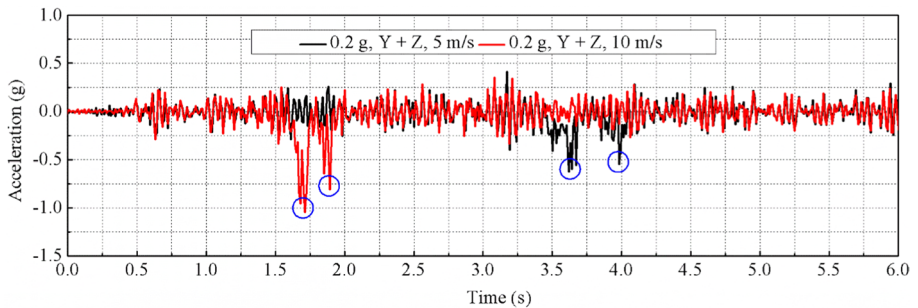**Fig. 13** Vertical girder-end acceleration of 5# girder

under uniform excitations, suggesting that, due to the effects of processing and installation precision, rails in the girder gap region have some initial irregularity, which significantly enhances the dynamic action of the train on rails in the girder gap region. When train speed increased from 5 to 10 m/s, the amplitude of the acceleration pulse rose from

Table 6 Maximum and minimum vertical seismic response of structures

| Components	Y + Z, 5 m/s		Y + Z, 10 m/s		D_1 (%)	D_2 (%)	D (%)
	Max	Min	Max	Min			
Vertical beam end acceleration (g)	0.416	−0.615	0.357	−1.047	17%	70%	70%
Vertical deformation of bearing at fixed end (mm)	0.061	−0.075	0.125	−0.128	105%	71%	105%
Vertical deformation of bearing at sliding end (mm)	0.075	−0.049	0.089	−0.126	19%	157%	157%
Vertical deformation of pier (mm)	0.023	−0.048	0.021	−0.066	10%	38%	38%
Vertical deformation of sliding layer (mm)	0.023	−0.039	0.086	−0.065	274%	67%	274%
Vertical deformation of CA mortar layer (mm)	0.037	−0.053	0.029	−0.054	28%	2%	28%
Vertical deformation of fastener (mm)	0.057	−0.039	0.062	−0.058	9%	49%	49%

0.616 to 1.047 g, and D reached 70%, revealing that train speed has a significant effect on the girder-end vertical acceleration of girders.

According to Fig. 14, the vertical deformation of all the structures (except the mortar layer) peaked upon the arrival of the train (1.5–2 s), and, for various structures, the vertical deformation at 10 m/s fluctuated more significantly than that at 5 m/s. If the train is deemed as an external excitation, the frequency corresponding to this excitation can be expressed as v/dv, where v and dv denote train speed and bogie center distance, respectively (Olmos and Astiz 2018). The bogie center distance of the train model was 1.75 m, so the excitation frequencies at 5 m/s and 10 m/s were 2.8 Hz, and 5.7 Hz, respectively. When the train passed the bridge model at a speed of 10 m/s, excitation frequencies were closer to the vertical first-order natural vibration frequency of structures, and the resonance phenomena induced were more significant. With increasing train speed, the train would engage in a more intense collision with structures when passing through girder gaps, for which the vertical deformation of structures would increase more significantly. In this test, high-stiffness screws were used as shear reinforcements between track slabs and base plates in the girder-end region, and their presence restrained the vertical deformation of the mortar layer. When the seismic excitation was 0.2 g, the D values of the vertical seismic responses of various structures at different train speeds all exceeded 28%, and the D values corresponding to the vertical deformation of the sliding-end bearing and the sliding layer reached 157% and 274%, respectively. Train speed clearly has a significant effect on the seismic vertical deformation of various structures, and track irregularity and train excitations make significant contributions to the vertical seismic deformation of structures.

4.2.2 Transverse seismic response

Figure 15 shows the transverse seismic deformation of structures at different train speeds, and Table 7 provides their maximum absolute values, where D denotes the difference in the responses at the two train speeds.

As can be seen from Fig. 15 and Table 7, the transverse deformation of the fixed-end and sliding-end bearings and piers at 10 m/s fluctuated more significantly than that at 5 m/s, mainly because the excitation frequency 5.7 Hz at 10 m/s was closer to the transverse first-order natural vibration frequency 8.3 Hz of the bridge model. On the other hand, a higher train speed produced more significant fluctuations in the vertical contact state of
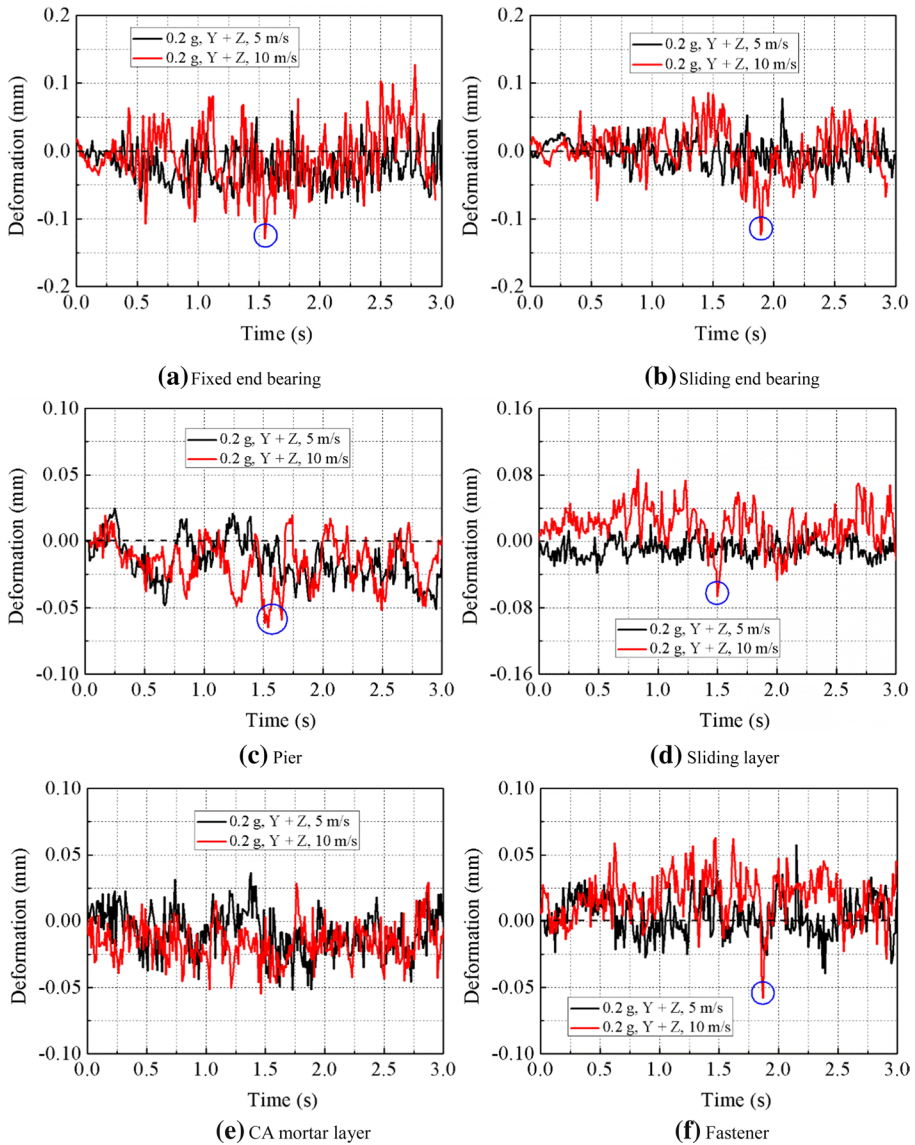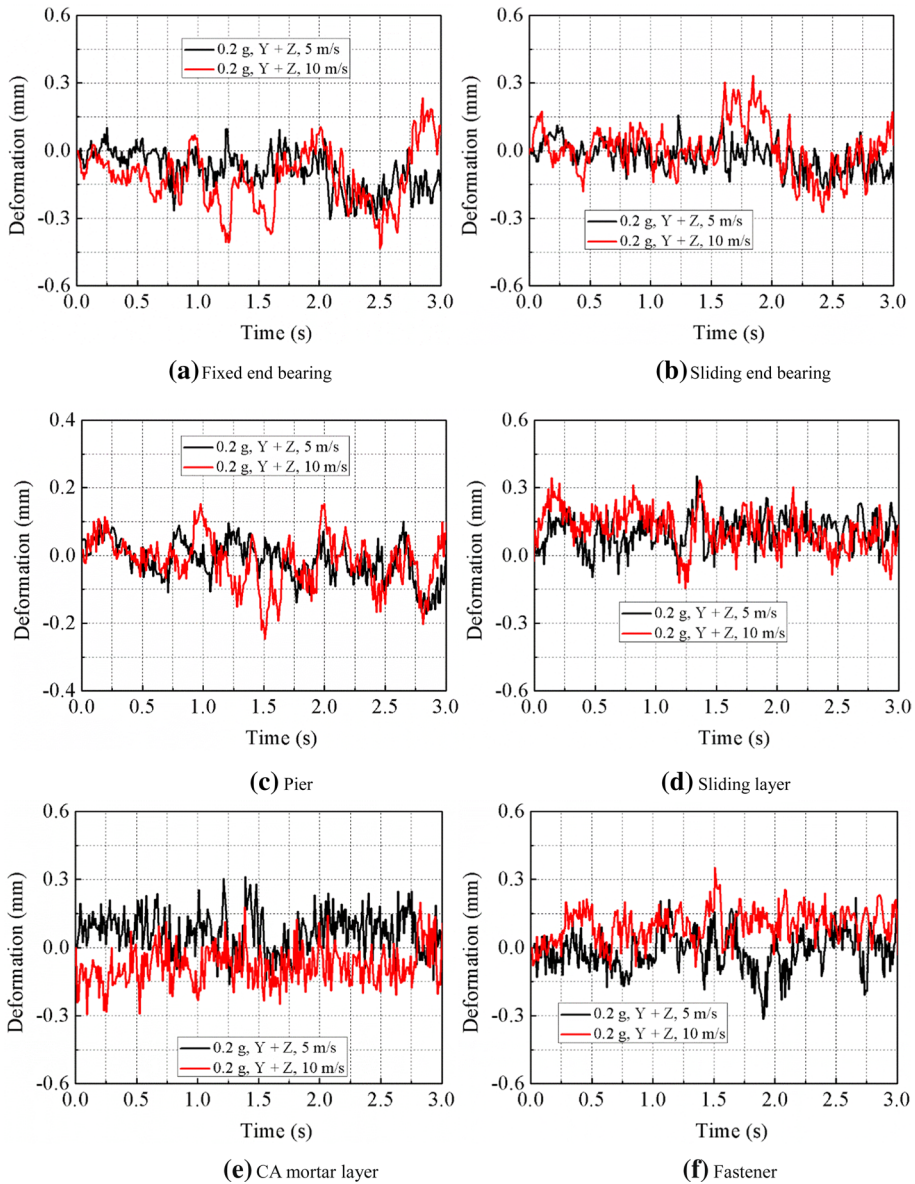
Fig. 14 Vertical deformation time history of the structures

bearings, and might even cause vertical separation between the bearing's upper plate and rubber. Because of the large mass of girders, the bearing's upper plate exerts a more violent impact on pot rings under horizontal seismic action, producing more significant deformation in these structures (Fig. 16). To be specific, the *D* values of the three reached 43%, 113%, and 45%, respectively, which makes clear that train speed has a significant effect on the transverse deformation of bearings and piers.

The deformation of the sliding layer, mortar layer, and fastenings was different in curve shape, but they had basically the same amplitude. This is because track structures and the

Fig. 15 Transverse deformation time history of the structures

train have a relatively small mass, the spring damping system of the train can reduce the transverse force applied by the train on rails to some extent, and the transverse force transferred by the train to track structures is limited. Taking base plates as an example, after coming into contact with lateral blocks, base plates could not continue to move, for which the sliding layer had roughly the same transverse deformation amplitude. The D values of the sliding layer, mortar layer, and fastenings were only 0.3%, 0.9%, and 3%, respectively,

Table 7 Maximum absolute values of the transverse structural seismic response

Components	Y+Z, 5 m/s	Y+Z, 10 m/s	D (%)
Transverse midspan acceleration (g)	0.440	0.293	50%
Transverse deformation of bearing at fixed end (mm)	0.308	0.440	43%
Transverse deformation of bearing at sliding end (mm)	0.156	0.332	113%
Transverse deformation of pier top (mm)	0.172	0.249	45%
Transverse deformation of sliding layer (mm)	0.349	0.346	0.9%
Transverse deformation of CA mortar layer (mm)	0.309	0.308	0.3%
Transverse deformation of fastener (mm)	0.328	0.339	3%
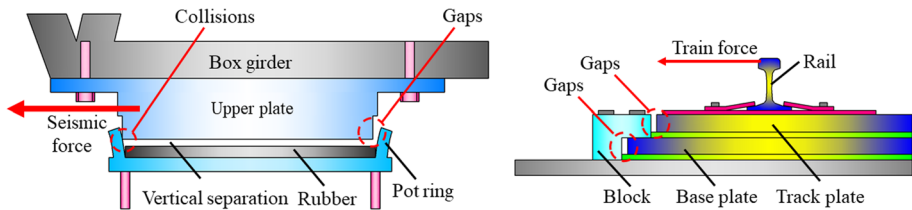
**Fig. 16** Bearing and track structural response during an earthquake

suggesting that the transverse action of the train does not produce any significant deformation in track structures, and the effect of train speed on the transverse deformation of track structures is negligible.

4.3 Effect of vertical component of ground motion on the vertical seismic response of structures

4.3.1 Vertical seismic response

To study the effect of the vertical component of ground motion on structural responses, the test speed was set as 10 m/s, bidirectional (transverse + vertical) and unidirectional (transverse) seismic excitations were input at the moment the train ran onto the bridge, and the vertical seismic responses of structures were recorded. Figures 17, 18 and Table 8 show vertical structural response time-histories under seismic action. According to Fig. 17, when the input of the vertical component of ground motion stopped, the amplitude of the girder-end pulse changed from 1.047 to 1.233 g, without any abrupt drop. This further confirms that the girder-end track irregularity of the bridge model is not induced by the vertical component of ground motion but is derived from the processing and installation errors of specimens and that train speed is the controlling factor influencing girder-end vertical acceleration. The D value of the girder-end pulse reached 18%, suggesting that the vertical component of ground motion may affect vertical wheel-rail contact state to a certain degree, causing differences in girder-end acceleration.

It can be seen from Fig. 18 and Table 8 that, when the vertical component of ground motion stopped, the amplitude of the vertical deformation of bearings dropped abruptly, and the D values of fixed-end and sliding-end bearings respectively reached
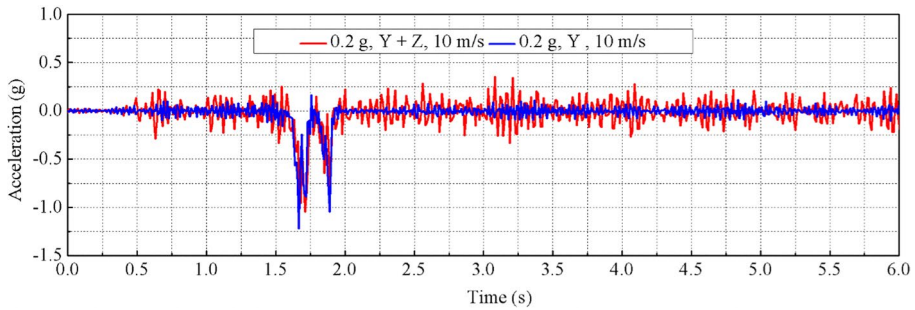
Fig. 17 Vertical girder-end acceleration of 5# girder

291% and 154%, indicating that the vertical component of ground motion makes a fairly significant contribution to the vertical deformation of bearings. Under vertical seismic action, the vertical deformation curve of bearings frequently showed high-amplitude positive values, meaning that the vertical component of ground motion may cause vertical separation between girders and bearings, resulting in secondary collision. The sliding layer and rails still maintained relatively significant vertical deformation. The reason is that, under uniform excitations, the earthquake-induced vertical deformation of track structures is relatively small, and the vertical deformation is primarily attributable to the train. The D values of the sliding layer, mortar layer, and fastenings respectively reached 37%, 41%, and 22%, suggesting that the vertical component of ground motion may have somewhat affected the contact state between the train and rails. The deformation curve of track structures showed positive values, regardless of the presence of vertical seismic action, indicating that the train may induce disengaging between track structures in the vicinity of girder gaps.

4.3.2 Transverse seismic response

Figure 19 shows the transverse seismic deformation of structures with and without the vertical component of ground motion, and Table 9 provides their maximum absolute values. According to Fig. 19, the transverse deformation of the fixed-end and sliding-end bearings and piers under bidirectional seismic excitations fluctuated more significantly than that under unidirectional seismic excitations, for a reason similar to that described in 3.2.2. That is, the vertical component of ground motion increases fluctuations in the vertical contact state of bearings, as well as bearings and piers experienced more significant deformation under horizontal seismic action. The D values of the three respectively reached 160%, 78%, and 32%, indicating that the vertical component of ground motion has a significant effect on the deformation of bearings and piers. In contrast, the deformation curves of the sliding layer, mortar layer, and fastenings had basically the same amplitude, primarily because the transverse force transferred by the train to track structures is limited. The D values of the sliding layer, mortar layer, and fastenings were 2%, 3%, and 4%, respectively, indicating that the effect of the vertical component of ground motion on the transverse deformation of track structures is insignificant.
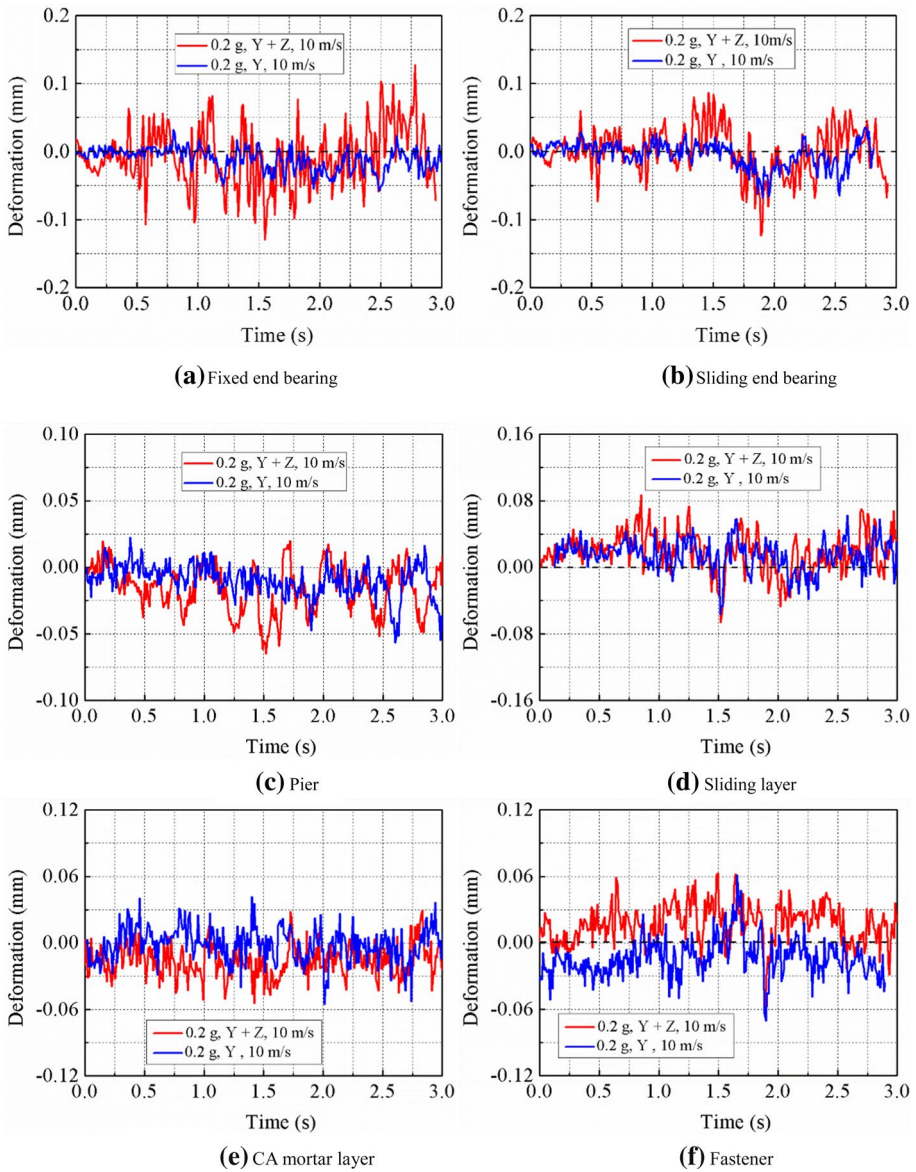
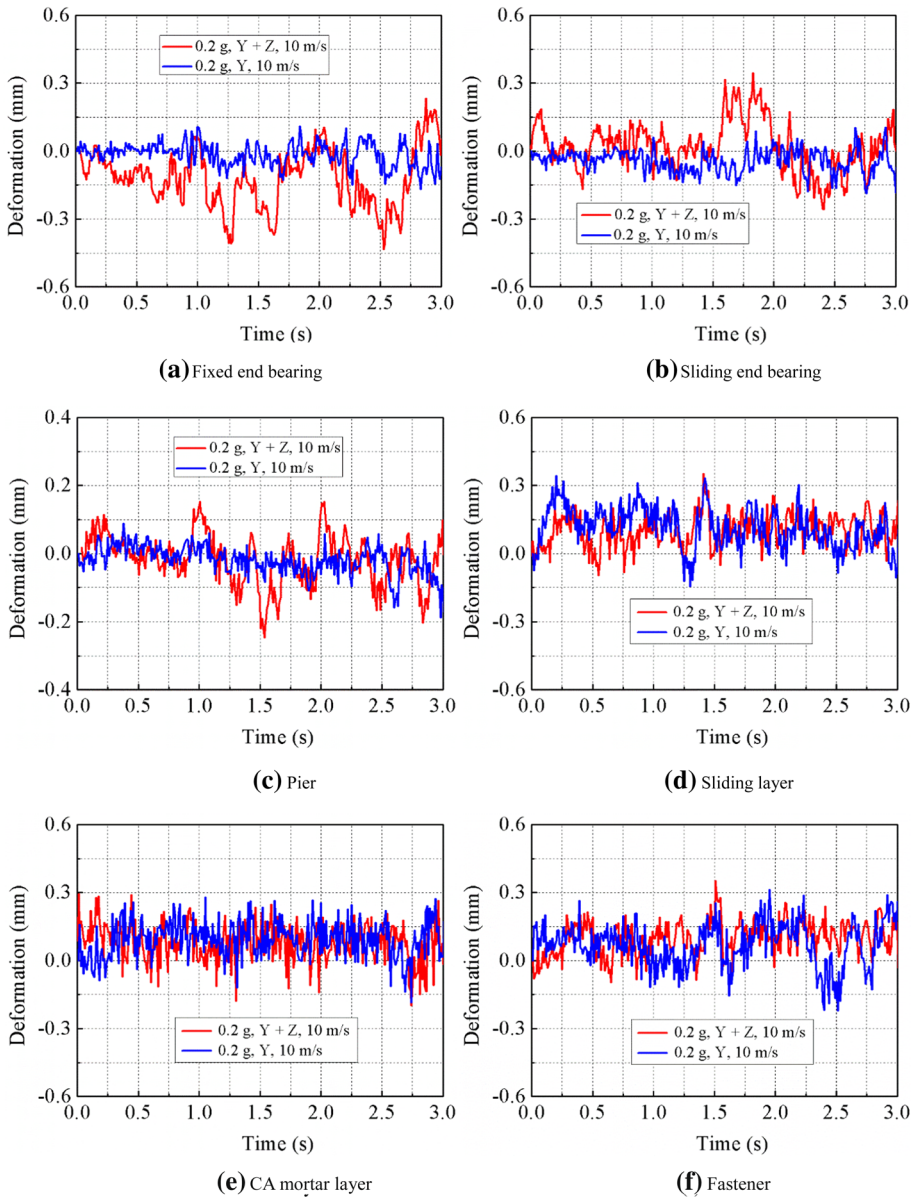**Fig. 18** Vertical deformation time history of the structures

Table 8 Maximum and minimum values of the vertical structural seismic response

Components	Y + Z, 10 m/s		Y, 10 m/s		D_1	D_2	D
	Max	Min	Max	Min			
Vertical beam end acceleration (g)	0.357	−1.047	0.175	−1.233	104%	18%	104%
Vertical deformation of bearing at fixed end (mm)	0.125	−0.128	0.032	−0.058	291%	121%	291%
Vertical deformation of bearing at sliding end (mm)	0.089	−0.126	0.035	−0.071	154%	77%	154%
Vertical deformation of pier (mm)	0.021	−0.066	0.024	−0.056	14%	18%	18%
Vertical deformation of sliding layer (mm)	0.086	−0.065	0.063	−0.057	37%	14%	37%
Vertical deformation of CA mortar layer (mm)	0.029	−0.054	0.041	−0.054	41%	0%	41%
Vertical deformation of fastener (mm)	0.062	−0.058	0.062	−0.071	0%	22%	22%

5 Conclusions

On the basis of building a reduced-scale model for a bridge and a train using a similarity ratio of 1:10 and constructing an on-bridge running test platform based on a four-array shaking table, this paper performs a running test under seismic action and explores the effects of train speed and the vertical component of ground motion on structural responses under the combined action of seismic and train loads. The main conclusions are as follows:

(1) A higher train speed leads to more intense wheel-rail interactions. Train speed is the controlling factor influencing girder-end vertical acceleration and has a significant effect on the vertical deformation of structures.

(2) The vertical component of ground motion significantly affects the vertical deformation of bearings and the inter-layer contact state of track structures, further affecting the deformation of track structures and wheel-rail interactions.

(3) Increasing train speed and the presence of a vertical component of ground motion significantly enhances the fluctuation effect of the vertical contact state of bearings, significantly intensifying the transverse seismic responses of bearings and piers.

(4) The transverse force applied by the train on track structures is insignificant. The effects of train speed and the vertical component of ground motion on the transverse deformation of track structures are negligible.

(5) The vertical component of ground motion may cause vertical separation between girders and bearings, resulting in secondary collision. Train excitations may induce disengaging between track structures in the vicinity of girder gaps.

Fig. 19 Transverse deformation time history of the structures

Table 9 Maximum absolute values of the transverse structural seismic responses

Components	Y + Z, 10 m/s	Y, 10 m/s	D
Transverse deformation of bearing at fixed end (mm)	0.440	0.169	160%
Transverse deformation of bearing at sliding end (mm)	0.332	0.186	78%
Transverse deformation of pier top (mm)	0.249	0.189	32%
Transverse deformation of sliding layer (mm)	0.346	0.340	2%
Transverse deformation of CA mortar layer (mm)	0.300	0.291	3%
Transverse deformation of fastener (mm)	0.339	0.326	4%

Declarations

Conflict of interest The authors declare that they have no known competing financial interests or personal relationships that could have appeared to influence the work reported in this paper.

References

Antolín P, Zhang N, Goicolea JM, Xia H, Astiz MÁ, Oliva J (2013) Consideration of nonlinear wheel-rail contact forces for dynamic vehicle-bridge interaction in high-speed railways. J Sound Vib 332(5):1231–1251. https://doi.org/10.1016/j.jsv.2012.10.022

Barone S, Calvi GM, Pavese A (2019) Experimental dynamic response of spherical friction-based isolation devices. J Earthq Eng 23(9):1465–1484. https://doi.org/10.1080/13632469.2017.1387201

Du XT, Xu YL, Xia H (2012) Dynamic interaction of bridge-train system under non-uniform seismic ground motion. Earthq Eng Struct D 41(1):139–157. https://doi.org/10.1002/eqe.1122

Furinghetti M, Pavese A, Quaglini V, Dubini P (2019) Experimental investigation of the cyclic response of double curved surface sliders subjected to radial and bidirectional sliding motions. Soil Dyn Earthq Eng 117:190–202. https://doi.org/10.1016/j.soildyn.2018.11.020

Gao C, Yuan X (2019) Development of the shaking table and array system technology in China. Adv Civ Eng 2019:1–10. https://doi.org/10.1155/2019/8167684

Guo W, Xia H, De Roeck G, Liu K (2012) Integral model for train-track-bridge interaction on the Sesia viaduct: dynamic simulation and critical assessment. Comput Struct 112:205–216. https://doi.org/10.1016/j.compstruc.2012.09.001

He X, Kawatani M, Hayashikawa T, Matsumoto T (2011) Numerical analysis on seismic response of Shinkansen bridge-train interaction system under moderate earthquakes. Earthq Eng Eng Vib 10(1):85–97. https://doi.org/10.1007/s11803-011-0049-1

Jangid RS (2001) Response of sliding structures to bi-directional excitation. J Sound Vib 243(5):929–944. https://doi.org/10.1006/jsvi.2000.3476

Jiang L, Kang X, Li C, Shao G (2019) Earthquake response of continuous girder bridge for high-speed railway: a shaking table test study. Eng Struct 180:249–263. https://doi.org/10.1016/j.engstruct.2018.11.047

Jiang L, He W, Wei B, Wang Z, Li S (2019) The shear pin strength of friction pendulum bearings (FPB) in simply supported railway bridges. B Earthq Eng 17(11):6109–6139. https://doi.org/10.1007/s10518-019-00698-x

Jiang L, Feng Y, Zhou W, He B (2019) Vibration characteristic analysis of high-speed railway simply supported beam bridge-track structure system. Steel Compos Struct 31(6):591–600. https://doi.org/10.12989/scs.2019.31.6.591

Jiang L, Zhang Y, Feng Y, Zhou W, Tan Z (2020) Simplified calculation modeling method of multi-span bridges on high-speed railways under earthquake condition. Bull Earthq Eng 18:303–2328. https://doi.org/10.1007/s10518-019-00779-x

Jiang L, Yu J, Zhou W, Yan W, Lai Z, Feng Y (2020) Applicability analysis of high-speed railway system under the action of near-fault ground motion. Soil Dyn Earthq Eng. https://doi.org/10.1016/j.soildyn.2020.106289

Kim CW, Kawatani M (2006) Effect of train dynamics on seismic response of steel monorail bridges under moderate ground motion. Earthq Eng Struct D 35(10):1225–1245. https://doi.org/10.1002/eqe.580

Kumar M, Whittaker AS, Constantinou MC (2015) Characterizing friction in sliding isolation bearings. Earthq Eng Struct D 44(9):1409–1425. https://doi.org/10.1002/eqe.2524

Liu Z, Jiang H, Zhang L and Guo E (2017) Natural Vibration Characteristics and Seismic Response Analysis of Train-Bridge Coupling System in High-Speed Railway. International Conference on Experimental Vibration Analysis for Civil Engineering Structures, 831–838

MRPRC (Ministry of Railways of People's Republic of China) (2009) Code for seismic design of railway engineering (in Chinese) (GB50111-2006). China Planning Press, China

Olmos J, Astiz M (2018) Non-linear vehicle-bridge-wind interaction model for running safety assessment of high-speed trains over a high-pier viaduct. J Sound Vib 419:63–89. https://doi.org/10.1016/j.jsv.2017.12.038

Pavese A, Furinghetti M, Casarotti C (2019) Investigation of the consequences of mounting laying defects for curved surface slider devices under general seismic input. J Earthq Eng 23(3):377–403. https://doi.org/10.1080/13632469.2017.1323046

Wei B, Wang P, Liu W, Yang M, Jiang L (2016) The impact of the concave distribution of rolling friction coefficient on the seismic isolation performance of a spring-rolling system. Int J Non Linear Mech 83:65–77. https://doi.org/10.1016/j.ijnonlinmec.2016.04.001

Wei B, Yang T, Jiang L, He X (2017) Effects of friction-based fixed bearings on the seismic vulnerability of a high-speed railway continuous bridge. Adv Struct Eng 21(5):643–657. https://doi.org/10.1177/1369433217726894

Wei F, Zhang Z, Liang G (2018) Study on shaking table array test of HSR train-track-bridge system under seismic action and velocity threshold of earthquake early warning. J China Railw Soc 40(3):101–106. https://doi.org/10.3969/ji.ssn.1001-8360.2018.03.01

Wei B, Zuo C, He X, Jiang L, Wang T (2018) Effects of vertical ground motions on seismic vulnerabilities of a continuous track-bridge system of high-speed railway. Soil Dyn Earthq Eng 115:281–290. https://doi.org/10.1016/j.soildyn.2018.08.022

Yang M, Meng D, Gao Q, Zhu Y, Hu S (2019) Experimental study on transverse pounding reduction of a high-speed railway simply-supported girder bridge using rubber bumpers subjected to earthquake excitations. Eng Struct 196:1–14. https://doi.org/10.1016/j.engstruct.2019.109290

Yu J, Jiang L, Zhou W, Liu X, Lai Z, Feng Y (2020) Study on the dynamic response correction factor of a coupled high-speed train-track-bridge system under near-fault earthquakes. Mech Based Des Struc. https://doi.org/10.1080/15397734.2020.1803753

Zhai W, Liu P, Lin J, Wang K (2015) Experimental investigation on vibration behaviour of a CRH train at speed of 350 km/h. Int J Rail Transp 3(1):1–16. https://doi.org/10.1080/23248378.2014.992819

Zhang N, Xia H, Roeck GD (2010) Dynamic analysis of a train-bridge system under multi-support seismic excitations. J Mech Sci Technol 24(11):2181–2188. https://doi.org/10.1007/s12206-010-0812-7

Zhang Z, Zhang Y, Lin J, Zhao Y, Howson WP, Williams FW (2011) Random vibration of a train traversing a bridge subjected to traveling seismic waves. Eng Struct 33(12):3546–3558. https://doi.org/10.1016/j.engstruct.2011.07.018

Zou S, Wenliuhan H, Zhou F (2019) Shaking table test of a high-speed railway bridge with a new isolation system. Eng Struct 196:1–12. https://doi.org/10.1016/j.engstruct.2019.109315

Publisher's Note Springer Nature remains neutral with regard to jurisdictional claims in published maps and institutional affiliations.